NUMERICAL AND EXPERIMENTAL ANALYSIS OF THE EFFECT OF WRINKLES ON THE RESIDUAL STRENGTH OF CURVED LAMINATES

Bruno Castanié, Pierre Journoud, Christophe Bouvet, Léon Ratsifandrihana

▶ **To cite this version:**

Bruno Castanié, Pierre Journoud, Christophe Bouvet, Léon Ratsifandrihana. NUMERICAL AND EXPERIMENTAL ANALYSIS OF THE EFFECT OF WRINKLES ON THE RESIDUAL STRENGTH OF CURVED LAMINATES. ECCM21 – 21st European Conference on Composite Materials, Jul 2024, Nantes (France), France. hal-04644695

HAL Id: hal-04644695

https://hal.insa-toulouse.fr/hal-04644695

Submitted on 11 Jul 2024

HAL is a multi-disciplinary open access archive for the deposit and dissemination of scientific research documents, whether they are published or not. The documents may come from teaching and research institutions in France or abroad, or from public or private research centers.

L'archive ouverte pluridisciplinaire **HAL**, est destinée au dépôt et à la diffusion de documents scientifiques de niveau recherche, publiés ou non, émanant des établissements d'enseignement et de recherche français ou étrangers, des laboratoires publics ou privés.

NUMERICAL AND EXPERIMENTAL ANALYSIS OF THE EFFECT OF WRINKLES ON THE RESIDUAL STRENGTH OF CURVED LAMINATES

P. Journoud[1], C. Bouvet[2], B. Castanié[3] and L. Ratsifandrihana[4]

[1] Institut Clément Ader (ICA), University of Toulouse, CNRS UMR 5312, INSA, ISAE-Supaéro, INSA, IMT Mines Albi, UPS, Toulouse, France
Email: journoud.pierre@gmail.com,
[2] Institut Clément Ader (ICA), University of Toulouse, CNRS UMR 5312, INSA, ISAE-Supaéro, INSA, IMT Mines Albi, UPS, Toulouse, France
Email: christophe.bouvet@isae-supaero.fr
[3] Institut Clément Ader (ICA), University of Toulouse, CNRS UMR 5312, INSA, ISAE-Supaéro, INSA, IMT Mines Albi, UPS, Toulouse, France
Email: castanie@insa-toulouse.fr
[4] Segula Aerospace & Defence, Segula Technologie – immeuble EQUINOX – bat. 1, 24 Boulevard Déodat de Severac, 31770 Colomiers, France
Email: Leon.RATSIFANDRIHANA@segula.fr

Keywords: Curved laminates, Defect, Wrinkles, L-angle, Bending

Abstract
An experimental study has been carried out to describe the evolution of the failure load relative to the maximum misalignment angle of curved carbon–epoxy laminates with out-of-plane wrinkle defects for a large range of misalignments. L-angle specimens with different levels of fibre wrinkling were manufactured and tested in four-point bending tests. To manufacture specimens with defects, two hand layup strategies were considered. In the first one, plies were directly stacked in the mould by hand with compaction, enabling parts to be made without defects. The second strategy involved stacking some or all of the layers on a flat surface first and then moving them into the mould. This second method promoted the appearance of wrinkles in the radius of curvature. Then, the specimens were subjected to four point bending tests. Increases in wrinkling levels led to decreases in failure loads. Then, a numerical model was developed to take wrinkle and local delamination defects into consideration and assess their impact on the failure load of the specimens. The wrinkles were modelled using the Discrete Ply Model strategy. The numerical model allowed the effects of each defect to be distinguished and their combined influence on the failure load to be studied.

1. Introduction

Composite part manufacturers or industries aiming to move to composite solutions are facing challenges in composite design [1]. Most of the time, designing composite is understood as, and limited to, the choice of stacking and sizing using the TSAI method or derivative, with or without an optimization scheme. Moreover, in practice it is also well known that “In composite, materials do not pre-exist the structure”, highlighting that a composite part is only obtained after a manufacturing phase, which depends on industrial constraints such as the scale of production, the certification requirements, the availability of materials, the size of the part, the cost, and many other constraints. In some particular cases, like corners (also called “clips”) used in fuselage, the effect of defect (wrinkles) must be taken into account in the sizing phase [2]. It is 1ocalized1 that wrinkles have significant influence on the mechanical properties of laminated composites and on their strength. Most of the works found in the literature focus on the effect of out-of-plane wrinkles on the strength of flat specimens under

compression tests [3,4] and only a few numbers deal with the effect of wrinkle defects in the radius of curvature on the mechanical properties, despite the fact that wrinkling is the most common defect on a curved specimen [5-10]. For this study, 42 specimens were produced by means of the two hand layup strategies described in Section 2 and [7]. The wrinkles were characterised by the maximum misalignment angle compared to the reference surface, which ranged from 5.3° to 83.3°. Then the L-shaped specimen were subjected to the four-point bending tests and the failure scenario was analyzed experimentaly and numericaly [5, 7-8].

2. Manufacturing of specimens with wrinkles

The tests were performed on L-Shaped CFRP specimens. The fibres and epoxy resin were respectively T700 and M21 (Hexcel Composites Company). The layup used was $[45_2/-45_2/90_2/0_2]_S$, so the 16 plies had a total theoretical thickness of 4.125 mm. This type of stacking with ± 45° plies as external plies is due to buckling considerations. It maximize the buckling load and is currently used in aeronautics.
The method used by Hu et al [11] is used and adapted here to produce specimens with different wrinkles magnitudes. This method involved stacking some or all of the layers (Fig. 1) on a flat surface first and then moving them into the mould. The proportion of plies stacked with this method has been outlined in red on Fig. 1. For instance, all sixteen plies of EP-1 were stacked with this strategy. For the EP-1/8 the first seven plies ($[45_2/-45_2/90_2/0]$) were stacked directly on the concave mould. Specimen EM-1 to EM-3 were stacked on a Convex mold. The dimensions of the pre-impregnated material used to manufacture each sample were 150 mm × 250 mm. After curing, each sample was cut into six specimens with an arm length of 113 mm and a width of 20 mm. Therefore, a total of 42 specimens shared among 5 manufacturing strategies of were tested in this study.

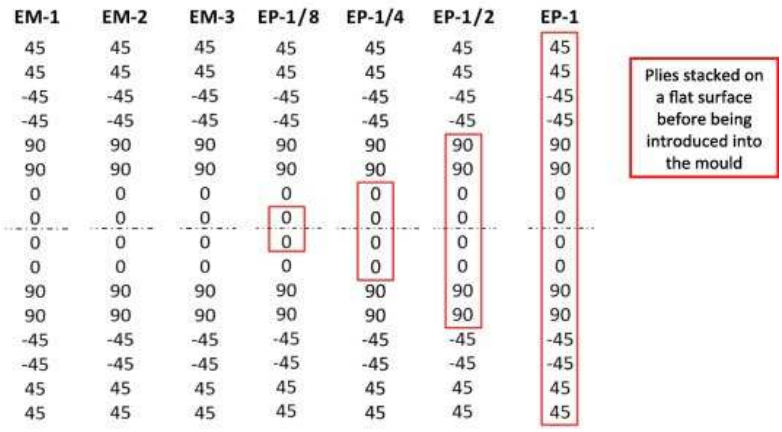

Figure 1. Strategies of hand layup used for the different specimens manufactured.

The calculation method of the misalignment angle θmax was described in [7] and results are shown in Fig. 2 . The values varies from 1.5° to 79°. Concerning the EP-1/4, EP-1/2 and EP-1 samples, the wrinkles seemed to be induced by the strategy of hand layup described earlier. The plies stacked on a flat surface before being introduced into the concave mould were subject to wrinkling, and so were all the plies stacked into the mould after them. It was observed that increasing the number of plies stacked on a flat surface increased the mean value of maximum misalignment angle with 38.4° for EP-1/4, 55.1°for EP-1/2 and 78.7°for EP-1. Moreover, EP-1/4 and EP-1/2 samples presented a greater scattering than the EP-1. Some voids were present in the EP-1/2 and EP-1 specimens, due to the high level of wrinkles located at the interface of 0° plies and at the interface between 0° and 90° plies in the lower part of the L-angle specimen in the case of EP-1/2. A piece of peel ply (symbolised in red on Fig. 8) was trapped under a wrinkle of the EP-1 specimens, consequently preventing the adhesion of the two inner parts of the wrinkles and creating a large defect. It is also noticeable that the specimens with the higher defects also exhibits delaminations areas.

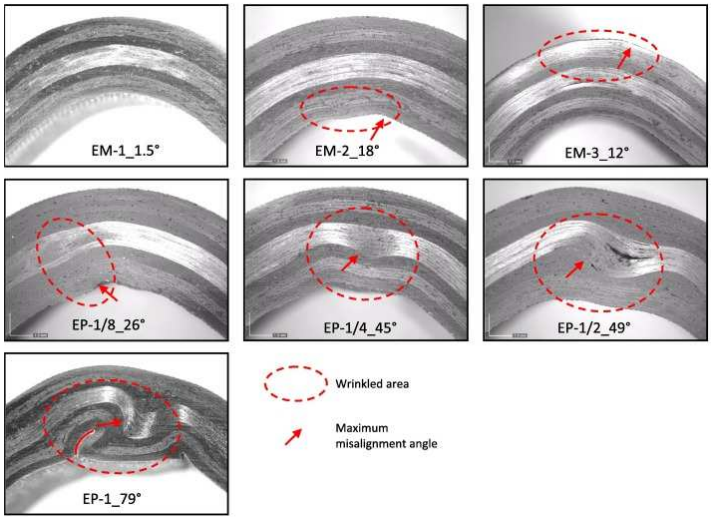

Figure 2. Example of wrinkles introduced in each batch of specimens.

Then the L-angles specimens were subjected to four point bending (Fig. 3 and Table 1)according to the procedure given in [5, 7-8]. In the following section a case will be detailed.

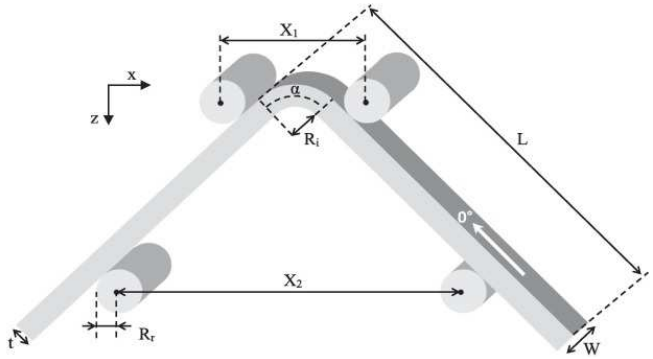

Figure 3. Configuration of the four-point bending test on L-angle specimen.

Table 1. Experimental setup characteristics, parameters, and L-angle specimen dimensions.

Thickness	Length	Width	Inner radius	Radius of cylindrical bars	Loading bars	Support bars
t (mm)	*L (mm)*	*w (mm)*	R_i *(mm)*	R_r *(mm)*	X_1 *(mm)*	X_2 *(mm)*
4.125	113	20	5.16	7.5	30	66

3. Numerical modelling of defects on L-angle specimens under four-point bending tests.

3.1. Discrete ply modeling

A complex 3D mesh following the orientation of each ply was used on the DPM to simulate the different failure modes (Fig. 3.). This model was already used and validated on many others subject like, among others, impact [12], large notches [13], 4 point bending of L-angle specimen [5] and will not be recalled extensively here. Volume elements used for the fibre failure were C3D8 and C3D6 for all orientations. Interface elements used for delamination and matrix cracking were classical cohesive zone model COH3D8 and COH3D6 elements. Interface elements used for matrix cracking were localised between two volume elements in the direction of the ply and interface elements used for delamination were localised at the interface of two adjacent plies. In fine, this modelling strategy requires only 15 material parameters, which are listed in Table 2. These parameters were found for T700/M21 for previous studies and are taken again here [5], [12-13].

Table 2. Material properties used in the DPM Modelling.

Density		**1600 Kg/m³**
Orthotropic elastic properties		
$E1t$	Tensile Young's modulus in fibre direction	130 000 MPa
$E1c$	Compressive Young's modulus in fibre direction	100 000 MPa
Et	Transverse Young's Modulus	7 700 MPa
$G1t=G1z$	In-plane shear modulus	4 750 MPa
Gtz	Out-of-plane shear modulus	2 900 MPa
$\nu 1t$	Poisson's ratio	0.3
Fibre failure		
$\sigma crush$	Mean longitudinal compressive crushing stress	250 MPa
$\varepsilon t0$	Tensile strain in fibre direction at damage initiation	0.016
$\varepsilon c0$	Compressive strain in fibre direction at damage initiation	−0.0125
$GIcf,T$	Critical energy release rate in mode I for tensile case	100 N/mm
$GIcf,C$	Critical energy release rate in mode I for compressive case	40 N/mm
Delamination		
$GIcdel$	Critical energy release rate in opening mode I	0.5 N/mm
$GIIcdel$	Critical energy release rate in shear mode II	1.6 N/mm
Matrix cracking		
σtf	Transverse tensile strength	50 MPa
$\tau 1tf$	In-plane shear strength	90 MPa

3.2. Modelling of specimens and consideration of the wrinkles

The entire specimen was meshed with elements of the same size, generated by an external script. The wrinkles were taken into account by a point statement, which was used to recalculate the position of the nodes corresponding to experimental interfaces previously measured on an image of the specimen side face obtained an during experiment. The new node coordinates ensured that all elements were orientated along the axis and passed through the theoretical origin of the radius of curvature. The modelling of wrinkles may lead to important modifications of the initial elements modelled and the variation of stiffness needs to be considered. On the example of Fig. 4, the modelling of the ply wrinkling has significant influence on the section of the volume element highlighted in red (Fig. 4.b) compared to the same element of the pristine specimen (Fig. 4.a). The section variation leads to a stiffness variation corresponding to a variation of fibre volume ratio. A coefficient, called *CoefS*, was calculated to correspond to the ratio between the initial section and the deformed section (Eq. (1)).

$$CoefS = S_{def}/S. \quad (1)$$

where S represents the initial section corresponding to the theoretical thickness of the ply and Sdef corresponds to the deformed section, which is calculated as the average of the four distances noted h_1,

h_2, h_3 and h_4 multiplied by the width of the element (perpendicular to the direction of the fibres, which remains constant for all elements) (Fig. 4): $S=Wh$ and $Sdef = W.(h_1 + h_2 + h_3 + h_4)/4$. The sections to be considered depend on the fibre directions (0°, 90° and ± 45°) [8]. The critical energy release rate for the fibers are also adapted [9].

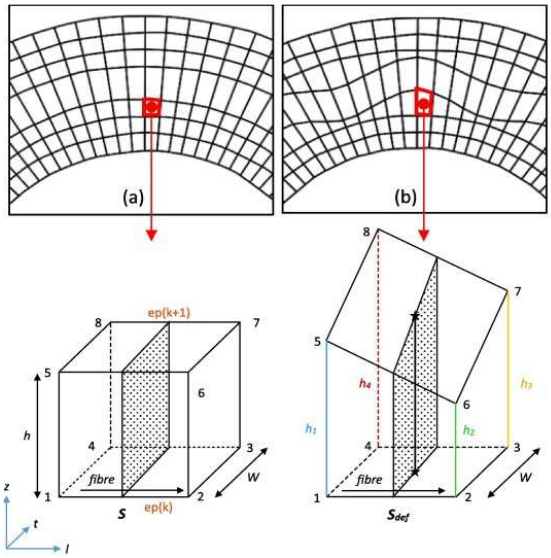

Figure 4. (a) 2D view of the mesh of a pristine specimen, indicating an initial volume element, (b) 2D view of the mesh of a specimen taking ply wrinkling into consideration, which points out a deformed volume element.

3.3. The case of an intermediate level of wrinkles without pre-delamination defect: EP-1/8_26°

The EP-1/8 batch of specimens were made in a concave mould and the two central plies at 0° were previously laid up by hand on a flat surface before being introduced into the mould. In this way, the mean value of maximum misalignment angle measurements was 26.4°. Nevertheless, it is worth noting that [45_2/-45_2/90_2/0_2] plies, in the lower part of the specimen, were affected by wrinkles. An image of the specimen was used to make a point statement of each interface between plies with different orientations. Then, it was used to modify the initial mesh of the specimen and take the wrinkling of some plies into consideration. The model produced by means of the point statement is represented in Fig. 5 and interfaces between plies are plotted in white on the experimental images, which were used for the measurements. This method allows perfectly realistic modelling of the wrinkles. Concerning the specimen studied in this part, the maximum misalignment angle measured relative to the reference surface was 26° and it is localised by a black circle in Fig. 5.

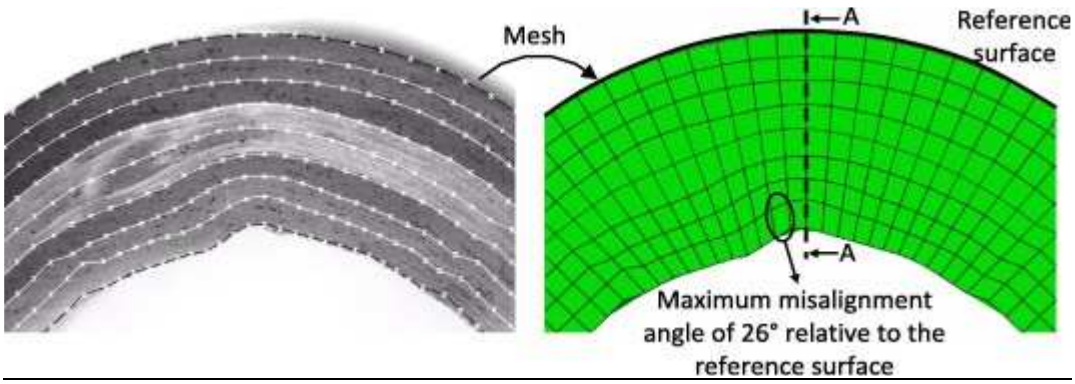

Figure 5. Comparison between experiment side face and meshed specimen EP-1/8_26°.

The experimental envelope of the load-machine displacement curve corresponding to the four-point bending tests conducted on the six specimens of the batch EP-1/8 is plotted on the graph of Fig. 6. The results show low variability regarding the stiffness and the failure load. The damage scenario is characterised by a first main load drop followed by a succession of smaller load drops due to the propagation of damage through the thickness of the specimen. Interested readers can refer to [7] for more information concerning the damage scenario of this specimen. The load-machine displacement curve corresponding to the simulation of the pristine specimen is plotted in dark blue. The light blue curve corresponds to the numerical model of the EP-1/8_26° specimen, which takes wrinkles into consideration as represented on Fig. 5.

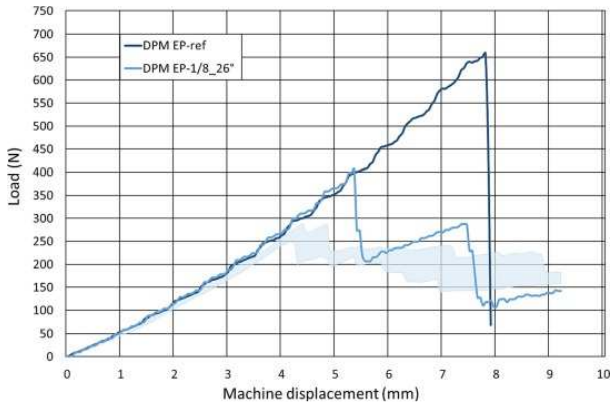

Figure 6. Load-Machine displacement curves of the EP-1/8_26° specimen and DPM modeling.

The simulation of the EP-1/8_26° specimen presented a failure load at approximately 400 N, which is 34% higher than the experimental mean failure load. The first load drop was driven by the delamination of the interfaces: [0/0], [90/0] and [-45/90] in the lower part of the specimen (Fig. 7) and matrix cracking of the 90° ply. This was due to out-of-plane tensile stress concentration around these plies in the middle of the specimen (Fig. 8). The stress concentration was maximal at the interface [-45/90] exactly as shown by the DIC on the experimental test of this specimen [7]. These damage occurrences were in agreement with the experimental ones reported on Fig. 7. The second load drop appeared at 290 N and 7.5 mm of machine displacement. It was due to the propagation of damage into the upper part of the specimen and, more particularly, to the delamination of the [90/-45] and [0/90] interfaces (Fig. 8). Matrix cracking was also present into the −45° and 90° plies, consistently with the experimental damage composed of matrix cracking in the 90° ply and delamination of the [90/-45] and [0/90] interfaces (Fig. 7).

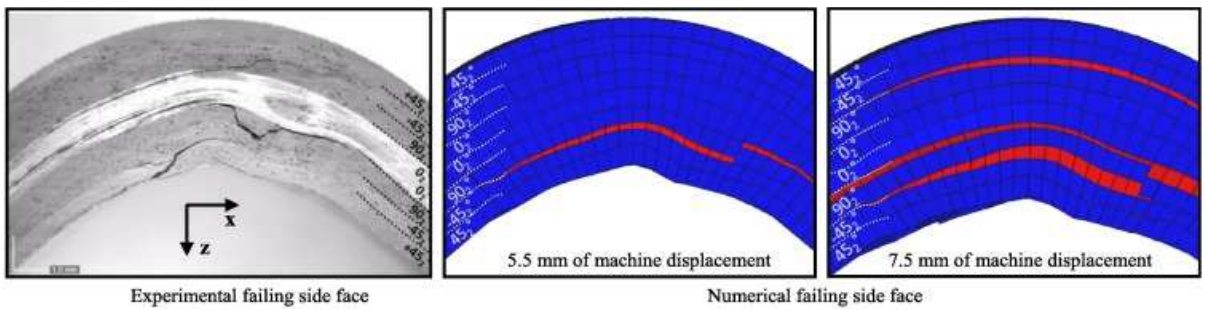

Figure 7. Comparison between experiment and numerical failure, side face.

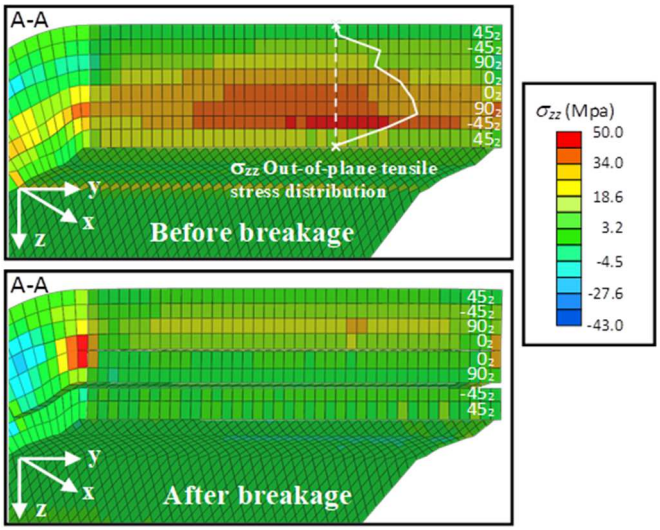

Figure 8. Stress through the section view A-A (defined in Fig. 5) of the specimen EP-1/8_26°.

Simulation considered only the wrinkling of the plies, which produced a failure load higher than expected, seeing the experimental results. In [7]it was shownthat initial delamination defects have a huge impact on the simulation in light of the pre-damaged area. In this case, no initial delaminations were visible on the specimen but internal initial delamination defects, porosity or other types of defects may have been present.

3. Conclusions

Based on experimental observations, a numerical model has been developed to take wrinkle defects into consideration on L-angle specimens under four-point bending tests. The load-machine displacement curve showed the same stiffness as with the pristine specimen but the failure load was dramatically affected by the presence of wrinkle defects, changing from 650 N to 406 N. Wrinkling regions induced an out-of-plane tensile stress concentration, which led to the failure of the specimen due to delaminations in its lower part. The failure loads provided by the DPM for the specimens modelled with wrinkles were 34% higher than the experimental mean value. This suggested that core initial delamination defects might be present through the width of this L-angle specimen.
In conclusion, the Discrete Ply Model allows wrinkle defects to be modelled. Simulations provide an acceptable correlation between experimental and numerical four-point bending tests on L-angle specimens with defects. Wrinkle defects are correctly estimated from experimental observations. The DPM could be used to simulate experimentally observed defects and qualify or disqualify the part. In conclusion, the localisation of wrinkle could have a major impact on the unfolding failure of curved specimens. It seems important to remember that, although the knockdown factors are important, these results could logically be expected due to the localisation of defects in the radius of the curvature of the curved specimen. Moreover, under four point-bending tests, induced stresses occur through the thickness, which explains their important influence on the failure load of curved specimens with defects. This model can be used to study different types of defects, even for flat parts, and to distinguish the most harmful.

References

[1] M.H. Hassan, A.R. Othman, S. Kamaruddin. A review on the manufacturing defects of complex-shaped laminate in aircraft composite structures. Int J Adv Manuf Technol, 91:4081-4094, 2017.
[2] F. Neveu, B. Castanié, P. Olivier. The GAP methodology: A new way to design composite structures. Mater Des 172: 107755, 2019.

[3] S. Mukhopadhyay, M.I. Jones, S.R. Hallett. Compressive failure of laminates containing an embedded wrinkle; experimental and numerical study. Compos Part A Appl Sci Manuf, 73:132-142, 2015.
[4] N. Xie, R.A. Smith, S. Mukhopadhyay, S.R. Hallett. A numerical study on the influence of composite wrinkle defect geometry on compressive strength. Mater Des, 140:7-20, 2018.
[5] P. Journoud, C. Bouvet, B. Castanié, F. Laurin, L. Ratsifandrihana. Experimental and numerical analysis of unfolding failure of L-shaped CFRP specimens. Compos Struct, 232:111563, 2020.
[6] Xu X., Jones M.I., Ali H., Wisnom M.R., Hallett S.R. Effect of out-of-plane wrinkles in curved multi-directional carbon/epoxy laminates. Compos Sci Technol, 197:108282, 2020.
[7] Journoud P., Bouvet C., Castanié B., Ratsifandrihana L. Experimental analysis of the effects of wrinkles in the radius of curvature of L-shaped carbon-epoxy specimens on unfolding failure. Comp Part A, 158: 106975, 2022.
[8] Journoud P., Bouvet C., Castanié B., Ratsifandrihana L. Numerical analysis of the effects of wrinkles in the radius of curvature of L- shaped CFRP specimens on unfolding failure. Comp Struct, 299:116107, 2022.
[9] Journoud P., Bouvet C., Castanié B., Ratsifandrihana L. Experimental and numerical compressive tests on curved laminate structures with embedded wrinkles. Mech Adv Mat Struct, 31(3):550–570, 2024.
[10] Journoud P., Bouvet C., Castanié B., Ratsifandrihana L. Effect of defects combined with impact damage on compressive residual strength in curved CFRP specimen. Thin-Walled Structures, 184:110484, 2023.
[11] H. Hu, D. Cao, Z. Cao, S. Li. Experimental and numerical investigations of wrinkle effect on failure behavior of curved composite laminates. Compos Struct, 261:113541, 2021.
[12] J. Serra, A. Trellu, C. Bouvet, S. Rivallant, B. Castanié, L. Ratsifandrihana. Combined loadings after medium velocity impact on large CFRP laminated plates: Discrete ply model simulations. Compos Part C, 6: 100203, 2021.
[13] J. Serra, C. Bouvet, B. Castanié, C. Petiot. Experimental and numerical analysis of Carbon Fiber Reinforced Polymer notched coupons under tensile loading. Compos Struct, 181 (2017), pp. 145-157.